Supporting Information

Facile construction of hierarchically porous carbon nanofibers modified by $FeCu/FeF_3$ heterojunction for oxygen electrocatalysis in liquid and flexible Zn-air batteries

Experimental section

Chemicals and materials

Silica sol ($SiO_2 \cdot H_2O$) was purchased form Beijing Deke Daojin Science And Technology Co., Ltd.. Ferric chloride ($FeCl_3$), Copper nitrate ($Cu(NO_3)_2$, 99%) and polyvinylpyrrolidone (PVP, Mw=1300000 g mol^{-1}) were purchased form Shanghai Aladdin Biochemical Technology Co., Ltd. Polytetrafluoroethylene emulsion (PTFE, Mw=678.10 g mol-1, 60 wt%) was bought from Jiangsu Transfar Technology co., LTD. All materials were purchased commercially and were used without further purification.

Synthesis of FeCu/FeF_3@HPCNFs

Firstly, a spinning solution consisting of 1.5 g polyvinylpyrrolidone (PVP, M_w=1300000 g mol^{-1}) and 10 g deionized water was mixed in a beaker with a magnetic stirrer for 30 min to obtain **solution A**. Then, 20 g of polytetrafluoroethylene emulsion (PTFE, 60wt%) and different molar ratios ($M(Fe^{3+})/M(Cu^{2+})$=3:1, 2:2 and 1:3) for ferric chloride and copper nitrate were added to the above mentioned solution and stirred for 3 h to obtain **solution B**. And during the stirring process, slowly add **solution B** to **solution A** and stir at room temperature for at least 3 h to avoid the formation of bubbles as much as possible. Finally, 2 mL of silica sol was added and stirred thoroughly for 1 h to obtain the final spinning solution. Subsequently, the obtained solution was transported to a self-built electro-blow spinning (EBS) apparatus for obtaining the precursor nanofibers at a voltage of 40 kV, a distance between the nozzle and the collector of 800 mm, and an air pressure of 0.1 MPa. Then the precursor nanofibers were placed to a muffle furnace and heated to 200℃ at a rate of 2℃ min^{-1} in an air atmosphere and maintained for 1 h. And the pretreated nanofibers were carbonized in a nitrogen atmosphere in a tube furnace by heating to 600 ℃ at a rate of 5℃ min^{-1} , then these nanofibers were heated to 800℃, 900℃ and 1000℃ respectively at a rate of 3℃ min^{-1}. Lastly, the sample was kept for 2 h at the carbonization temperature. The prepared porous carbon nanofibers loaded with various heterojunction FeCu/FeF_3 can be obtained with different molar ratios

($M(Fe^{3+})/M(Cu^{2+})$=3:1, 2:2 and 1:3), which named as the prepared $Fe_{0.75}Cu_{0.25}/FeF_3$@HPCNFs, FeCu/FeF_3@HPCNFs and $Fe_{0.25}Cu_{0.75}/FeF_3$@HPCNFs. Meanwhile, the samples with only added iron salts were marked as Fe@HPCNFs. The samples with only copper salts added were marked as Cu@HPCNFs. For the convenience of writing, samples without adding iron and copper salts were recorded as the HPCNFs. And the samples without adding iron salts, copper salts, and silica sol were recorded as PCNFs.

Material characterization

The morphologies of various samples are tested using field emission scanning electron microscopy (FE-SEM) with a Hitachi S4800 instrument at a test voltage of 10–20 kV. The internal morphologies and structures of various samples are examined using transmission electron microscopy (TEM) with a Hitachi H7650 instrument. The single fiber morphology of the sample and the lattice spacing of the crystals can be clearly observed using field emission high-resolution transmission electron microscopy (HR-TEM, JEM-F200) to determine the compositions of the prepared materials. The Brunauer-Emmett-Teller (BET) surface area can be determined using a Micromeritics ASAP-2020 nitrogen adsorption apparatus. The crystal structure of the sample also is characterized using X-ray diffraction (XRD) with a BRUKER D8 ADVANCE instrument. The chemical composition of the sample is tested and analyzed using the X-ray photoelectron spectroscopy (XPS) with a Thermo Fisher USA instrument.

Electrochemical measurements

The electrochemical measurements were conducted through using an electrochemical cell equipped with a spinner supplied by the PINE Co. And the related electrochemical performances can be tested based on the CHI760E electrochemical workstation of Shanghai Chenhua Company. The working electrodes mainly included rotating disk electrode (RDE) with a 5 mm glassy carbon (GC) disk, rotating ring disk electrode (RRDE) with a 5.61 mm GC disk and a 7.09 mm platinum ring. The applied Hg/HgO electrode was used as the reference electrode, and the

carbon rod was used as the counter electrode. All potentials are reported relative to a reference hydrogen electrode (RHE). For the ORR tests, we used a 0.1 M potassium hydroxide (KOH) solution as the electrolyte. For the OER tests, a 1 M KOH solution was used. The used catalyst ink was prepared by mixing 4 mg catalyst, 40 μL Nafion solution, 250 uL N, N-dimethylformamide and 250 uL deionized water, with a functional catalyst loading of 0.5 mg cm^{-2} for RDE and RRDE tests.

At the same time, in the assembled Zn-air cells, high-grade zinc flakes were used as the cell anode, and the prepared hydrophobic carbon papers coated with catalyst ink (1 mg cm^{-2}) were regarded as the cell cathode. The applied liquid electrolyte was the mixed material including 6 M KOH and 0.2 M $Zn(Ac)_2$. The charge-discharge cycle stability of the assembled battery was evaluated through a series of 5-min charge and 5-min discharge cycles.

Computational methods

The Vienna Ab Initio Simulation Package (VASP) is utilized for conducting density functional theory (DFT) calculations. These calculations incorporated the generalized gradient approximation (GGA) and employed the spin-polarized Perdew–Burke–Ernzerhof (PBE) functional for the exchange-correlation potential. The electron-ion interactions are modelled using the projector augmented wave method, with a plane-wave energy cut-off set at 380 eV. Structural optimization adhered to a convergence criterion of 10^{-4} eV for energy difference and 0.02 eV $Å^{-1}$ for force differences per atom. For negating the interactions between adjacent surfaces, a vacuum spacing exceeding 15 Å is introduced. System energy and electronic density of states (DOS) are calculated based on a single-point energy difference of 10^{-6} and a Gamma-grid K-points configuration of 3×2×1. For achieving more accurate energy estimations, a simplified (rotationally invariant) approach to DFT+U, as proposed by Dudarev *et al.*, is employed[S1-S2]. The "U–J" values are set at 4 for Fe and 4.5 for Cu, following pertinent literature[S3-S4].

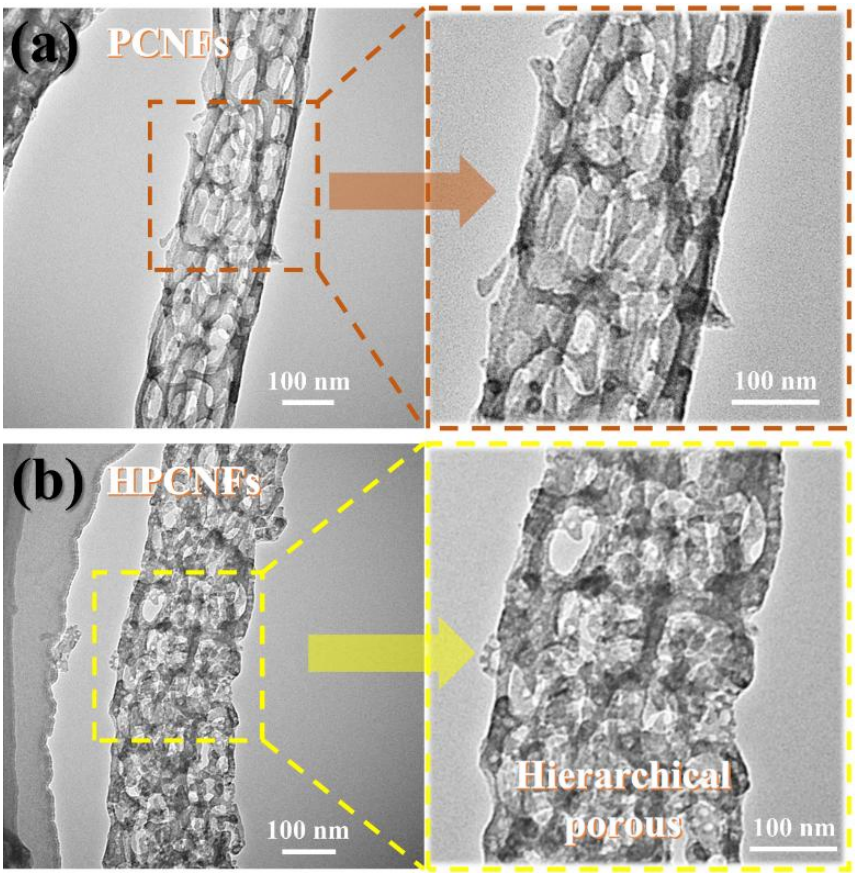

Fig. S1. (a) TEM images of PCNFs and **(b)** HPCNFs

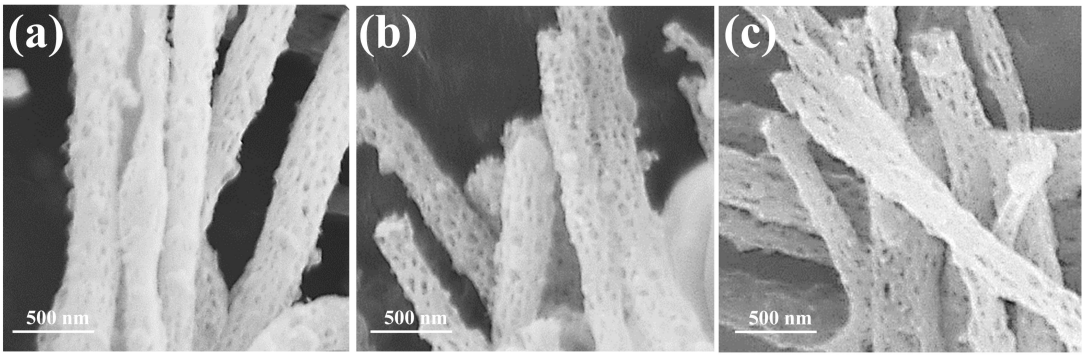

Fig. S2 The SEM images of FeCu/FeF_3@HPCNFs based on various carbonization temperatures of **(a)** 800 ℃, **(b)** 900 ℃ and **(c)** 1000 ℃

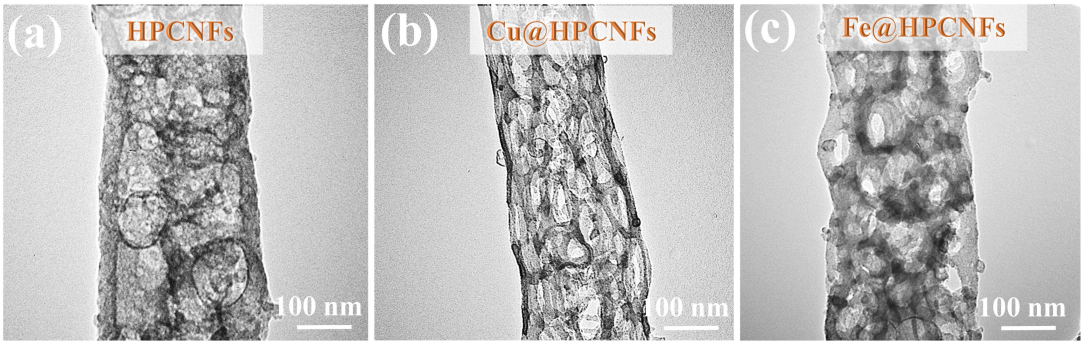

Fig. S3 The TEM images of **(a)** HPCNFs, **(b)** Cu@HPCNFs and **(c)** Fe@HPCNFs.

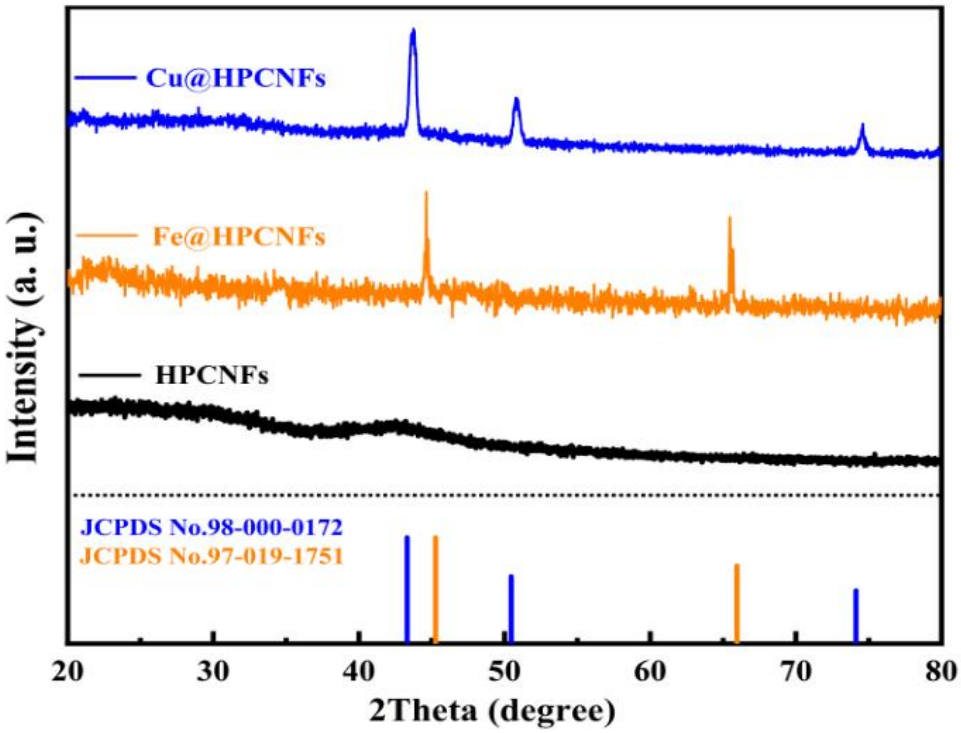

Fig. S4 The XRD patterns of HPCNFs, Cu@HPCNFs and Fe@HPCNFs.

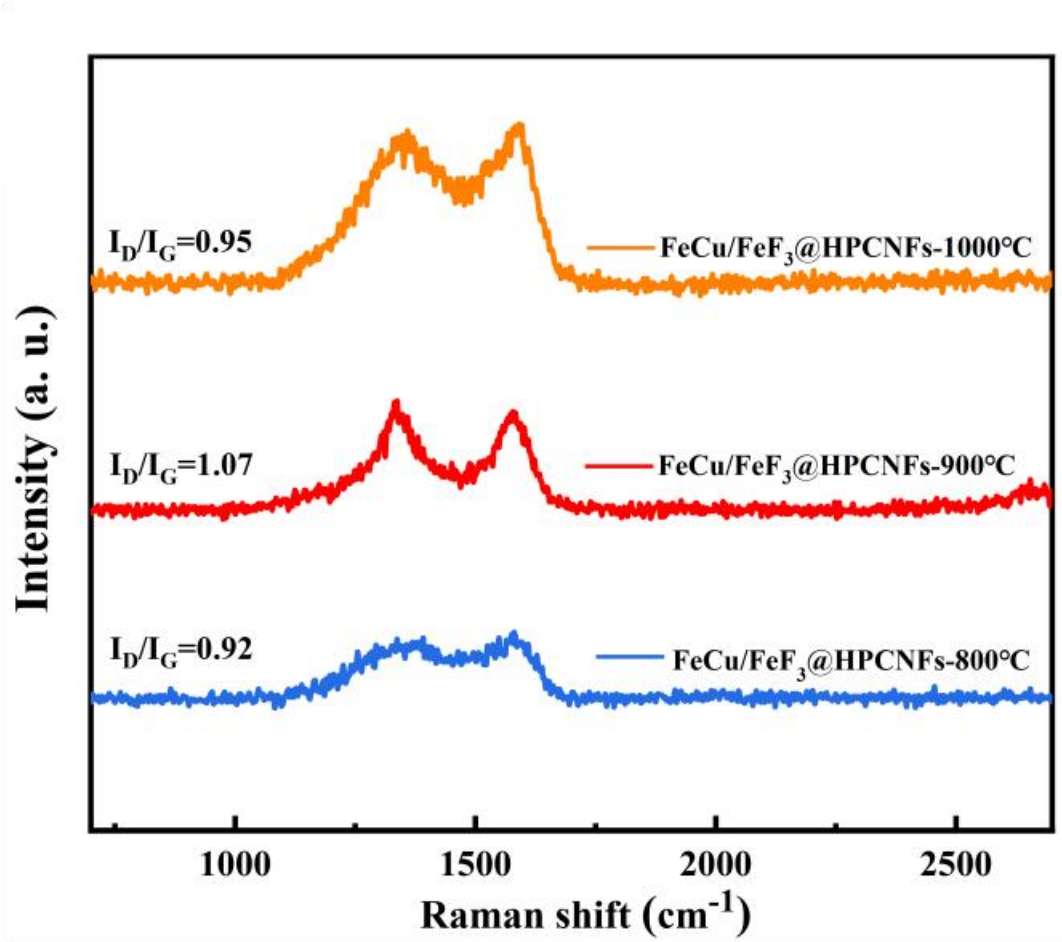

Fig. S5 The Raman spectra of FeCu/FeF_3@HPCNFs based on various carbonization temperatures of 800℃, 900℃ and 1000℃.

.

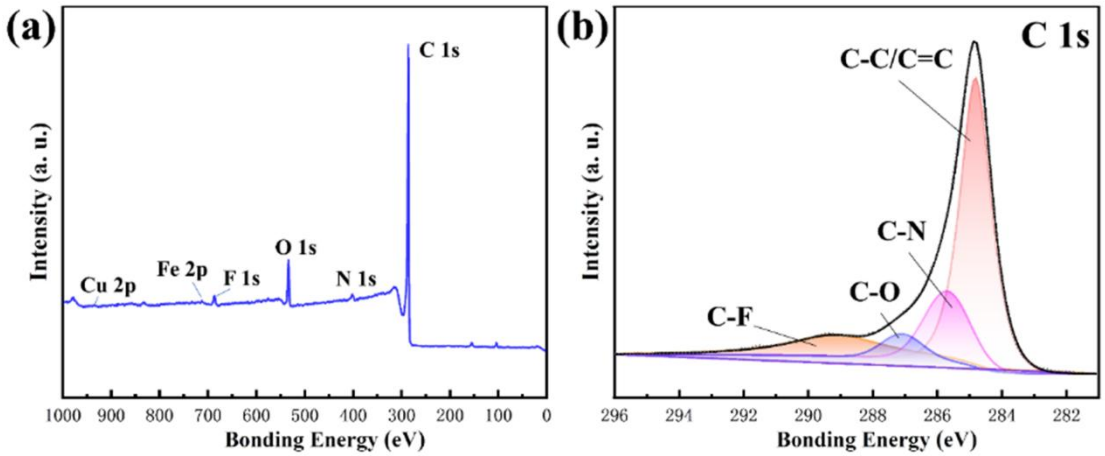

Fig. S6 (a) The full-spectrum of FeCu/FeF_3@HPCNFs **(b)** The high resolution XPS spectra of C 1s

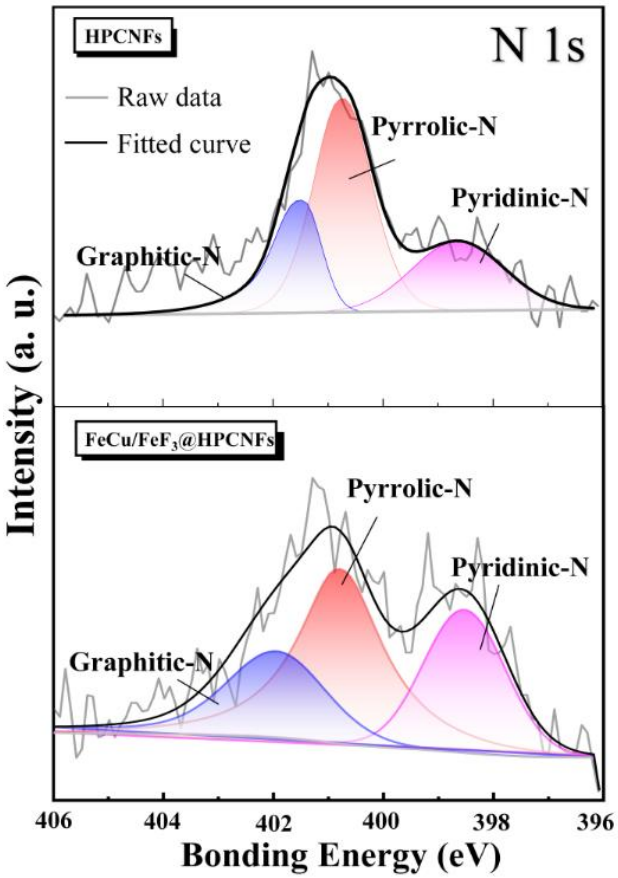

Fig. S7 The comparison of N 1s spectra of HPCNFs and FeCu/FeF_3@HPCNFs (Normalized treatment)

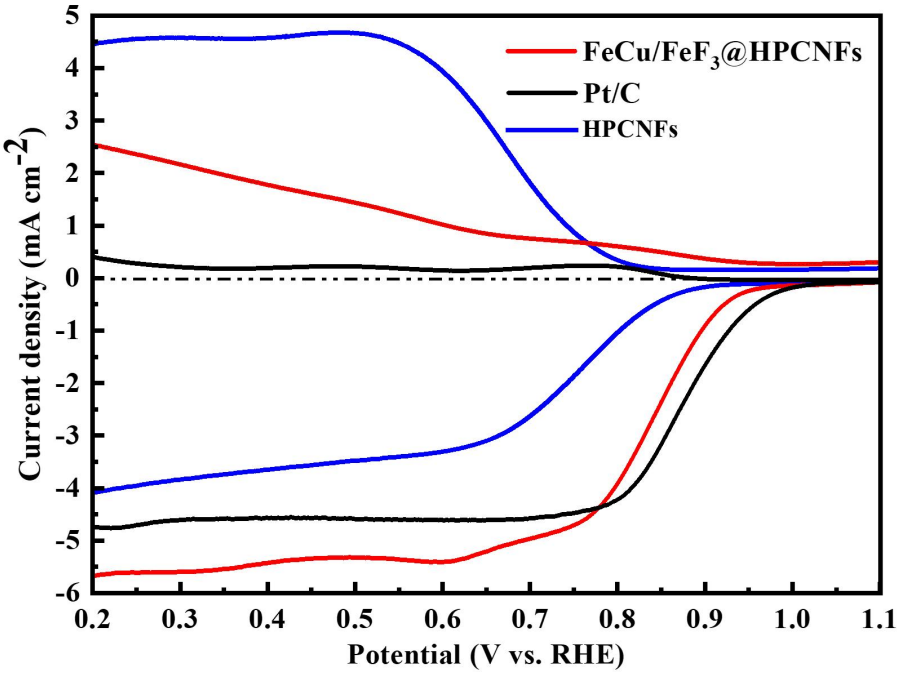

Fig. S8 The LSV curves obtained using RRDE testing of various samples.

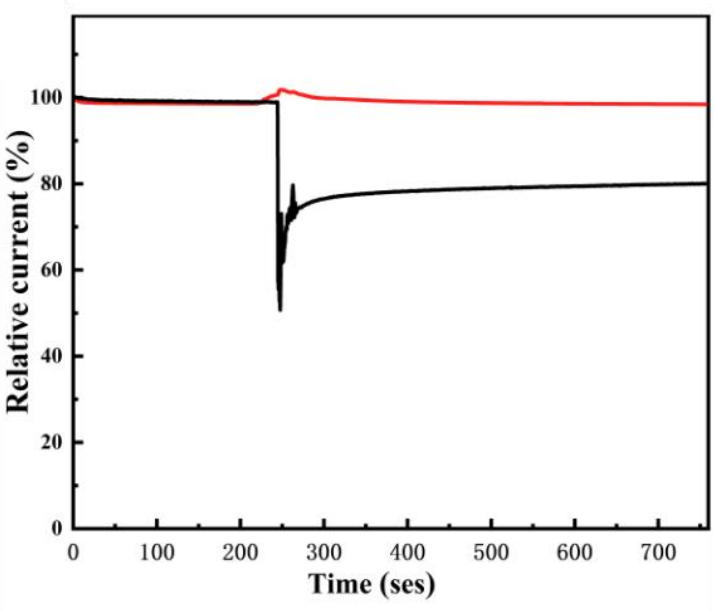

Fig. S9 The methanol tolerance test of various electrocatalysts.

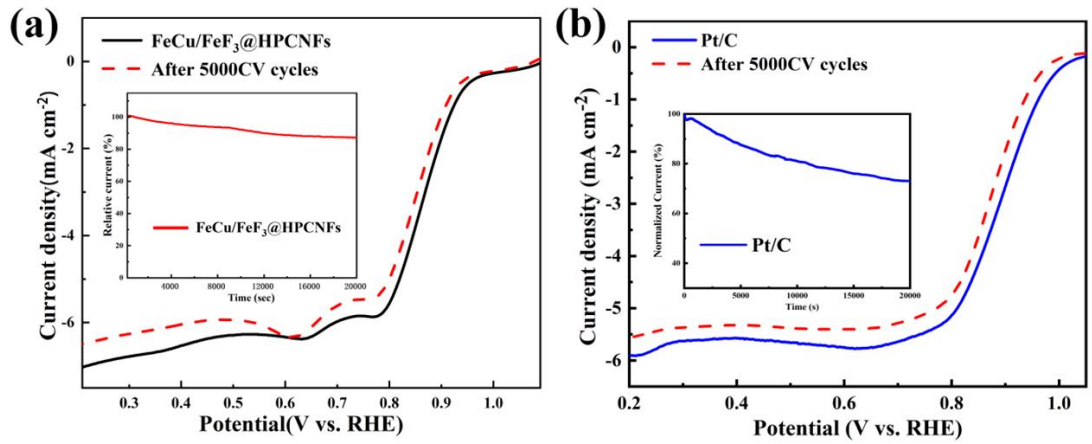

Fig. S10 (a) The polarization curves before and after 5000 cycles and **(b)** chronoamperometric (i-t) of FeCu/FeF_3@HPCNFs and Pt/C.

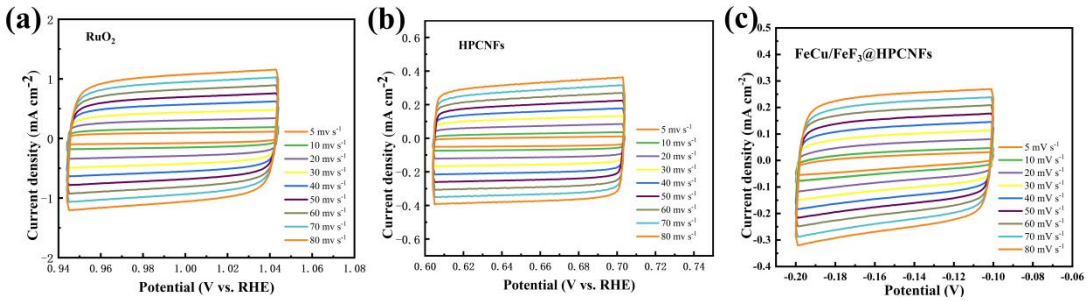

Fig. S11 The cyclic voltammetry(CV) curves ofRuO_2**(a)**, HPCNFs **(b)** and $FeCu/FeF_3$@HPCNFs **(c)** with various scan rates (5-80 mV s^{-1})

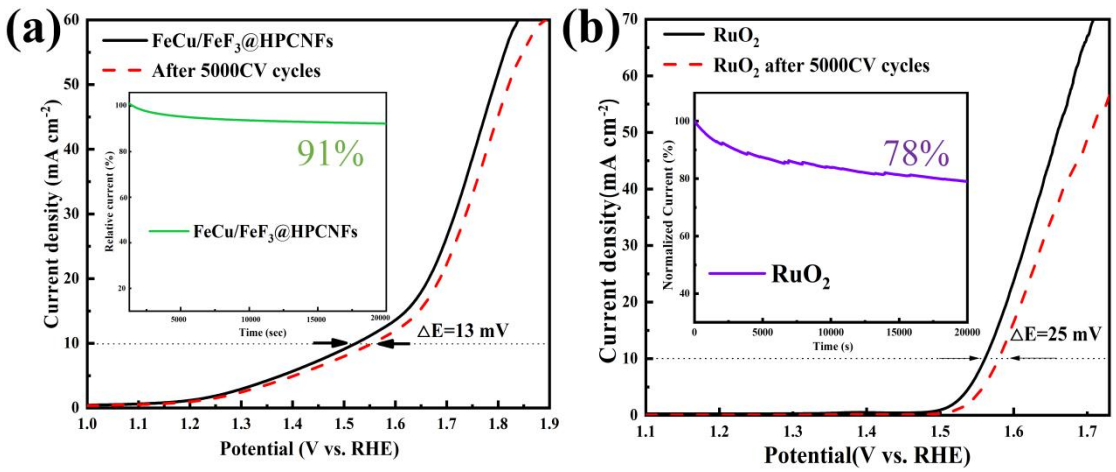

Fig. S12 The stability test chart of **(a)** FeCu/FeF_3@HPCNFs and **(b)** RuO_2.

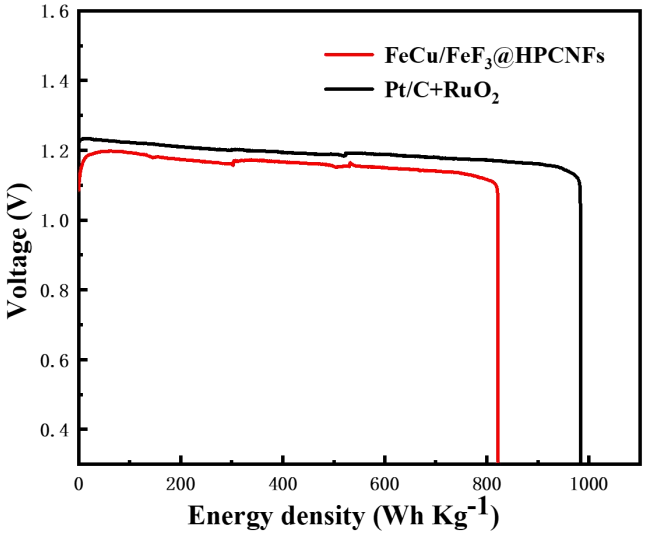

Fig. S13 Energy density curve of various assembled cells

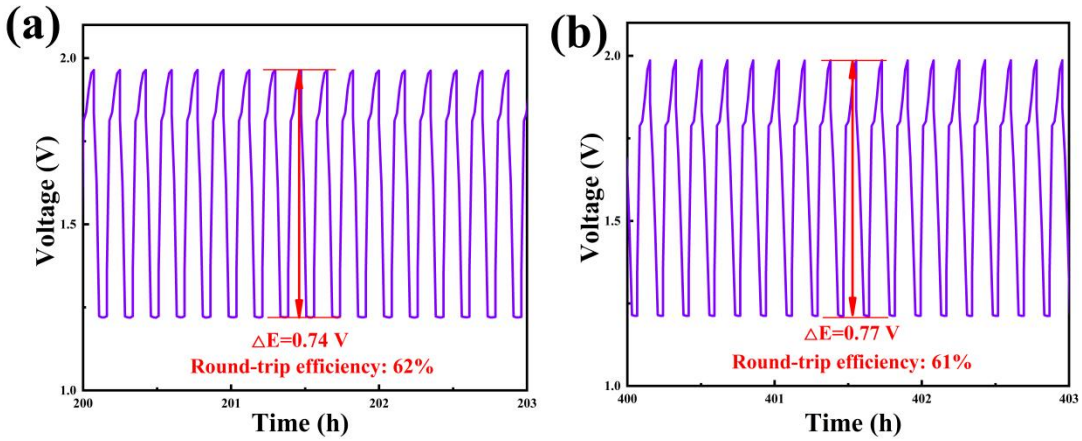

Fig. S14 The round-trip efficiency of ZABs assembled based on FeCu/FeF_3@HPCNFs during different periods.

Table S1 The specific surface area based on different sample tests.

Catalysts	SSA (m^2/g)
$Fe_{0.75}Cu_{0.25}/FeF_3$@HPCNFs	887
$Fe_{0.25}Cu_{0.75}/FeF_3$@HPCNFs	869
FeCu/FeF_3@HPCNFs	**959**
Cu@HPCNFs	635
Fe@HPCNFs	720
HPCNFs	756
PCNFs	591

Table S2 Comparison of ΔE ($E_{j=10}$-$E_{1/2}$) and peak power density of ZABs with Ni-based electrocatalysts.

Sample	ΔE [V]	Peak power density of ZAB [mW cm^{-2}]	Reference
IE-NiCoFe/HPLIG	0.663	163	[S5]
DN-CP@G	0.987	135	[S6]
CNTs-NC-CCC	0.78	68	[S7]
FeCo/FeCoNi@NCNTs-HF	0.758	156.22	[S8]
CoNi/BCF	0.8	155.1	[S9]
CoN/FeN@N,S-C-800	0.74	168.3	[S10]
Fe–NiNC-50	0.73	220	[S11]
Co_3O_4@x-HoNPs@HPNCS-60	0.74	94.1	[S12]
CNF@Zn/CoNC	0.88	140.1	[S13]
NiFe@C@Co CNFs	0.749	130	[S14]
CoP@PCNF	0.67	124	[S15]
FeS_2–CoS_2/NCFs	0.76	257	[S16]
CoFe/N CNFs	0.67	149	[S17]
FeCo/FeCoNi@NCNTs-HF	0.758	156.22	[S18]
FeCu/FeF_3@HPCNFs	**0.64**	**192**	**This work**

Reference

[S1] V.I. Anisimov, J. Zaanen, O.K. Andersen, Band theory and mott insulators: Hubbard U instead of stoner I[J]. Physical Review B-Condensed Matter, 1991, 44(3): 943-954.

[S2] S.L. Dudarev, G.A. Botton, S.Y. Savrasov, et al. Electron-energy-loss spectra and the structural stability of nickel oxide: An LSDA+U study[J]. Physical Review B-Condensed Matter, 1998, 57(3): 1505-1509.

[S3] S. Kattel, B. Yan, Y. Yang, et al. Optimizing binding energies of key intermediates for CO_2 hydrogenation to methanol over oxide-supported copper[J]. Journal of the American Chemical Society, 2016, 138(38): 12440-12450.

[S4] V. Alexandrov, K.M. Rosso, Ab initio modeling of Fe(II) adsorption and interfacial electron transfer at goethite (alpha-FeOOH) surfaces[J], Physical Chemistry Chemical Physics, 2015, 17(22): 14518-14531.

[S5] Sha, Y.; Peng, Y.; Huang, K.; *et al.* 3D binder-free integrated electrodes prepared by phase separation and laser induction (PSLI) method for oxygen electrocatalysis and zinc-air battery. Advanced Energy Materials, 2022, 12 (25): 2200906.

[S6] Hang, C.; Zhang, J.; Zhu, J.; *et al.* In situ exfoliating and generating active sites on graphene nanosheets strongly coupled with carbon fiber toward self-standing bifunctional cathode for rechargeable Zn-air batteries. Advanced Energy Materials, 2018, 8 (16): 1703539.

[S7] Zheng, X.; Qian, Y.; Gong, H.; *et al.* Bridge-linking interfacial engineering of triple carbons for highly efficient and binder-free electrodes toward flexible Zn-air batteries. Applied Catalysis B: Environmental, 2022, 319: 121937.

[S8] Wang, Z.; Ang, J.; Zhang, B.; *et al.* FeCo/FeCoNi/N-doped carbon nanotubes grafted polyhedron-derived hybrid fibers as bifunctional oxygen electrocatalysts for durable rechargeable Zinc-air battery. Applied Catalysis B: Environmental, 2019, 254: 26-36.

[S9] Wan, W.; Liu, X.; Li, H.; *et al.* 3D carbon framework-supported CoNi nanoparticles as bifunctional oxygen electrocatalyst for rechargeable Zn-air batteries, Applied Catalysis B: Environmental, 2019, 240: 193-200.

[S10] Ren, S.; Duan, X.; Lei, M.; *et al.* Energetic MOF-derived cobalt/iron nitrides

embedded into N, S-codoped carbon nanotubes as superior bifunctional oxygen catalysts for Zn-air batteries. Applied Surface Science, 2021, 569: 151030.

[S11] Zhu, X.; Zhang, D.; Chen, C.-J.; *et al.* Harnessing the interplay of Fe-Ni atom pairs embedded in nitrogen-doped carbon for bifunctional oxygen electrocatalysis, Nano Energy, 2020, 71: 104597.

[S12] Ji, D.; Fan, L.; Tao, L.; *et al.* The kirkendall effect for engineering oxygen vacancy of hollow Co_3O_4 nanoparticles toward high-performance portable Zinc-air batteries. Angewandte Chemie International Edition, 2019, 58 (39): 13840-13844.

[S13] Zhao, Y.; Lai, Q.; Zhu, J.; *et al.* Controllable Construction of core-shell polymer@zeolitic imidazolate frameworks fiber derived heteroatom-doped carbon nanofiber network for efficient oxygen electrocatalysis. Small, 2018, 14 (19): 1704207.

[S14] Chen, X.; Pu, J.; Hu, X.; *et al.* Janus Hollow nanofiber with bifunctional oxygen electrocatalyst for rechargeable Zn-air battery. Small, 2022, 18 (16): 2200578.

[S15] Deng, N.; Zeng, Q.; Feng, Y.; *et al.* CoP Nanoparticles embedded in three-dimensional porous network-like structured N, O co-doped carbon nanofibers as an effective bi-functional electrocatalyst for rechargeable Zinc-air batteries. Catalysis Science & Technology 2023, 13 (16): 4823-4838.

[S16] Shi, X.; He, B.; Zhao, L.; *et al.* FeS_2-CoS_2 Incorporated into nitrogen-doped carbon nanofibers to boost oxygen electrocatalysis for durable rechargeable Zn-air batteries. Journal of Power Sources, 2021, 482: 228955.

[S17] Chen, X.; Pu, J.; Hu, X.; *et al.* Confinement synthesis of bimetallic MOF-derived defect-rich nanofiber electrocatalysts for rechargeable Zn-air battery. Nano Research, 2022, 15 (10): 9000-9009.

[S18] Wang, Z.; Ang, J.; Zhang, B.; *et al.* FeCo/FeCoNi/N-doped carbon nanotubes grafted polyhedron-derived hybrid fibers as bifunctional oxygen electrocatalysts for durable rechargeable Zinc-air Battery. Applied Catalysis B: Environmental, 2019, 254: 26-36.